Modeling the mechanical behavior of Articular Cartilage via Molecular Dynamics: a simplified computational approach

Luca-Barbu Agarici
s-5058295

Faculty of Science and Engineering

Period:15/04/2025-30/06/2025

Bachelor's Project

1^{st} Examiner:[PhD Andrea Giuntoli, Faculty of Science and Engineering]

2^{nd} Examiner:[Dr. P.K.Sharma, Faculty of Medical Sciences]

Daily Supervisor:[PhD Student Akram Abbasniabazeh, Faculty of Science and Engineering]

Contents

university of groningen / faculty of science and engineering / biomedical engineering

Appendix: Declaration on the use of generative AI systems during BME projects

Title of the project:	Modeling the mechanical behavior of Articular Cartilage via Molecular Dynamics: a simplified computational approach
Your full name:	Agarici Luca-Barbu
Student number:	s5058295

In the project I have used systems based on generative artificial intelligence (AI)[1, 2]
(please check one of the boxes with X).

☒ Yes ☐ No

If you have selected "Yes", complete the rest of the form. If you have selected "No", simply fill in the place, date and signature below.

I have used the following generative AI based systems in the creation of this thesis: [1, 2]
(please list all systems used below)

1.	ChatGPT
2.	
3.	
Other:	

I further declare that I
(please check one of the boxes with X).)

- ☐ have actively informed myself about the capabilities and limitations of the above-mentioned AI systems to the extent that I can use them responsibly,
- ☐ have labelled the content taken from the AI systems listed above with my details in the table below,
- ☐ have verified that the content generated by the above-mentioned AI systems and adopted by me is factually correct,
- ☒ am aware that, as the author of this work, I am responsible for the information and statements made in it,
- ☐ am aware that the violation of the disclosure of the use of generative AI in my work is a deception and leads to an evaluation with an insufficient grade.

- Indicate in the table on the next page when the above-mentioned AI systems have been used during your project.
- When you have completed and signed the form, please add it to the beginning of your thesis/report, straight after the standard title page).

[1] This declaration does not apply to the use of basic widely used tools for checking spelling and grammar, translating texts and improving software quality for data analysis and software prototypes.
[2] If you are unsure whether an IT system used is a generative AI system and/or whether you need to declare it, declare it.

Page 1 of 4

Figure 1: First page of the AI usage declaration

university of groningen / faculty of science and engineering / biomedical engineering

I have applied the above-mentioned AI systems as indicated below.

Areas of contribution	Number AI system(s) used	Description of the manner of use and compliance with good scientific practice, if necessary separately by chapter of the work
Development and conception of the research project	0	
Collection and evaluation of literature sources	0	
Elaboration, collection and/or procurement of data	0	
Processing of data	0	
Selection of methodology	0	

Figure 2: Second page of the AI usage declaration

university of groningen / faculty of science and engineering / biomedical engineering

Programming	1	I have used ChatGPT to improve the code for one of the plots I have in the thesis. It was strictky used to improve the quality of the aspect of the plots. The processing of the data part of the code was strictly written by myself and with the help of my daily supervisor.
Analysis/evaluation of the data/sources	0	
Interpretation of the analysis /evaluation and derivation of conclusions	0	
Writing of the manuscript: Creation of visualizations	0	
Writing of the manuscript: Structuring the text	0	
Writing of the manuscript: Formulation of text	0	

Figure 3: Third page of the AI usage declaration

university of groningen / faculty of science and engineering / biomedical engineering

Writing of the manuscript: Revision of text	0	

Further contributions / additional information:

Place	Date	Signature
Groningen	07/07/2025	

Page 4 of 4

Figure 4: Fourth page of the AI usage declaration

Abstract

Understanding the mechanical behavior of biological tissues is essential for advancing both medical research and clinical practice. Among these tissues, articular cartilage stands out due to its unique anisotropic and depth-dependent structure, which enables it to perform critical functions such as load distribution and joint lubrication. However, this same complexity makes it difficult to study through experimental methods alone, due to its small size, structural heterogeneity, and limited regenerative capacity imply significant challenges. To address these limitations, computational modeling has emerged as a powerful tool for simulating cartilage behavior under various mechanical conditions. This thesis presents a simplified model designed to capture key features of cartilage, including density and stiffness changes. Through tensile and compressive loading simulations, the model is evaluated for its ability to sustain mechanical deformation similar to real cartilage. Although the model is simplified, it is still representative of showcasing how the tissue behaves. We found that our structure, due to its anisotropy, distributes the load mostly in the bottom layer, and during the deformation, it is crucial that the fibers are allowed to rearrange to better withstand the stress. This ability is heavily influenced by the stiffness and the density of crosslinking. These findings establish a foundation for more advanced, biologically detailed simulations. In the long term, such models could enable patient-specific analyses and support the design of targeted treatment strategies. This work lays the groundwork for future computational studies aimed at advancing our understanding of cartilage biomechanics and expanding our knowledge of our tissues.

Chapter 1

Introduction

The human body is a great model of biological engineering—an adaptive, self-regulating system composed of diverse, hierarchically organized structures. From the macroscopic coordination of organ systems to the microscopic intricacies of cellular interactions, the body exemplifies a delicate balance between structure and function. Its ability to withstand mechanical forces, recover from injury, and maintain homeostasis is rooted in the unique mechanical properties of its tissues.

Mechanical integrity is an essential factor in the performance of how the human body operates. Tissues such as bone, tendon, ligament, and cartilage are not only biological but also mechanical constructs. These tissues enable mobility, provide support, and protect internal organs. Their capacity to sustain loads, distribute forces, and deform without damage is central to human health. To appreciate the biomechanical function of these tissues, one must understand a key material characteristic often found in biological structures: anisotropy [1].

Anisotropy, in a mechanical context, refers to the directional dependence of material and structural properties. Unlike isotropic materials, where mechanical behavior such as stiffness or strength is the same in all directions, anisotropic materials exhibit variations depending on the direction of applied force. This property is not incidental in biology. It is an evolved trait, reflective of how tissues are used and loaded in the body. For example, tendons are stiff along their length but compliant transversely, enabling them to transmit muscle forces efficiently to the bones and joints while remaining flexible [2]. Similarly, bones exhibit varying degrees of stiffness and toughness based on their orientation and location, allowing them to withstand complex loading scenarios with remarkable resilience [3].

Among the many anisotropic tissues in the body, articular cartilage is particularly notable for its structural and functional complexity. It acts as a force and friction absorber for our knees and joints. Its homeostasis is based on a continuous change in deformation, which allows the flow of nutrients in and out of the tissue. The unique mechanical properties of cartilage are largely derived from its extracellular matrix. Each zone contains a specific alignment of collagen fibers and distribution of proteoglycans, which contribute to the tissue's depth-dependent anisotropy. This anisotropic architecture is essential for the proper functioning of cartilage; however, it also renders it vulnerable to damage when mechanical loading surpasses physiological thresholds—such as in cases of trauma, repetitive motion, or pathological conditions. When the cartilage deteriorates, it permits the direct contact of bones, resulting in discomfort and a

diminished range of motion [4]. This progression may ultimately culminate in osteoarthritis, a degenerative ailment that can severely compromise one's mobility.

Experimental investigation of cartilage mechanics has provided significant insights over the decades. However, the layered and anisotropic nature of cartilage, combined with its thin geometry and location within joints, imposes substantial challenges for direct testing. Traditional mechanical testing can be invasive and may not accurately capture localized deformations or microstructural damage. Moreover, biological variability and the difficulty of isolating specific variables complicate the interpretation of experimental data.

To address these limitations, the field has increasingly turned to computational simulations as an alternative approach. Computational modeling enables researchers to construct virtual representations of cartilage tissue, incorporating its geometric, material, and structural characteristics. Through simulations, it is possible to apply controlled loading conditions, systematically vary parameters like stiffness and cross-linking density and keep track of stress distribution, bond breakage, and tissue failure. These tools offer powerful means to explore the internal mechanics of cartilage and test hypotheses that would be difficult or would require a great amount of resources to examine experimentally [5].

The present work builds upon this foundation, aiming to deepen our understanding of how anisotropic mechanical properties influence cartilage behavior under mechanical loading. Thus, this study focuses on evaluating the behavior of a simplified model of cartilage to determine how closely it mimics the mechanical responses of the native tissue. The analysis involves several structural features, including fiber density, orientation, and overall mechanical performance. Our findings revolve around the effect of anisotropy on the structure. The bottom layer supports most of the load in both deformations. The fiber orientation in comparison with the load distribution aligns well with the literature. Additionally, stiffness increase can dictate a structure that does not allow for reorientation of its fibers to better sustain the load. While the model does not yet capture the full complexity of biological cartilage, it serves as an essential foundational step toward developing a comprehensive and physiologically accurate simulation framework. Additionally, such a model could be adapted for patient-specific applications, enabling targeted treatment planning and advancing research efforts. This approach has the potential to significantly accelerate the development of diagnostic tools and therapeutic strategies.

Chapter 2

Background Literature

In this chapter, we will dive in detail on the properties of cartilage and the principles of the mechanical tests.

2.1 Anatomy of Cartilage

Cartilage is a soft tissue that has load-bearing functions and it is present all over the body. As a dense connective tissue, it consists mainly of collagen, proteoglycans (PG) and chondrocytes. The organization of these components, along with the mechanical properties of cartilage, varies zonally [6]. The concentration, orientation and position of collagen network, the entrapped proteoglycans aggregates and water molecules determine the mechanical properties of the cartilage tissue, providing tensile strength and compressive resilience based on electrostatic repulsion forces [7]. Cartilage experiences a variety of applied loads, such as compression, shear, friction and tension.

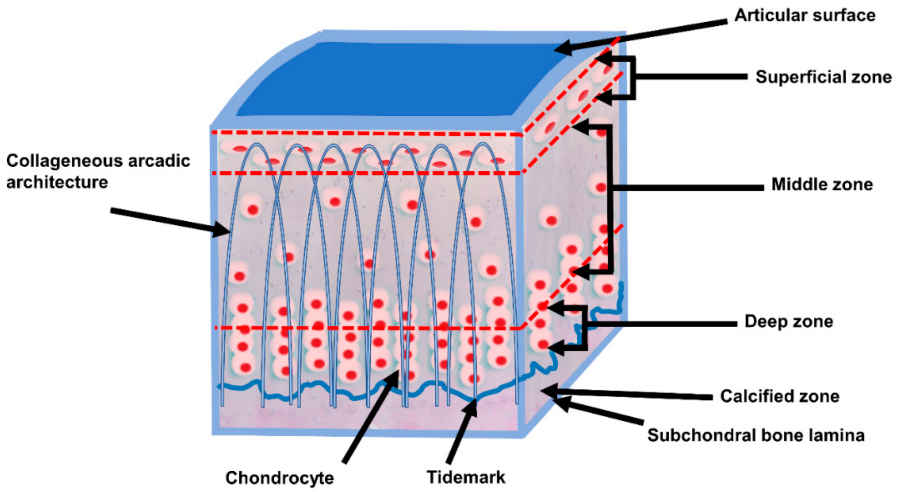

Figure 2.1: Cross-sectional diagram of healthy cartilage and cellular organization in the layers of cartilage. In the superficial layer collagen fibers are orientated horizontally, in the middle zone randomly orientated, and in the deep zone are orientated vertically [12,13,14].

Cartilage shows a zonal arrangement depicted in Figure 2.1, specifically, it is divided into

three zones with different types of biomechanical and biochemical behavior. The superficial zone is the thinnest layer with the highest water content. It is composed of tightly packed collagen fibers oriented parallel to the surface of the structure. This ensures a smooth surface appropriate for joint movement while adding resistance to shear and tensile stresses [8]. The middle zone is characterized by thicker collagen fibers compared to the superficial zone. They are arranged in an oblique fashion around chondrocytes. In this zone, they have a lower density and a spheroid shape [9]. This layer produces resistance to compressive forces [10]. The deep zone contains collagen fibers that are perpendicular to the cartilage surface and the highest concentration of PG. In addition, it contains the lowest number of spheroidal chondrocytes out of all zones. Together, they provide the greatest amount of resistance to compressive forces [10].

2.2 Mechanical properties

The mechanical attributes of a material are its mechanical characteristics in different conditions and under various external loads [11]. They represent the ability of a material to be molded into a suitable shape. To better visualize those properties, we will use a stress-strain relationship

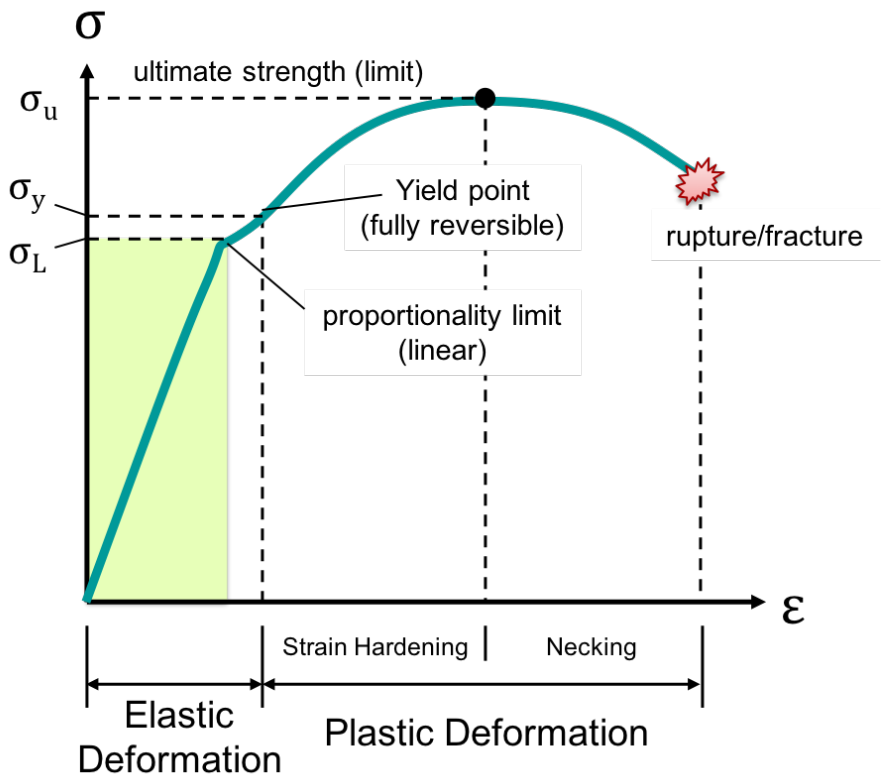

Figure 2.2: Stress-Strain relationship curve alongside the main events of the mechanical behavior of a material [16].

curve in our results. As a general example, Figure 2.2 presents a stress-strain curve with its key points. The linear or elastic region is the amount of deformation and stress the material

can sustain without any permanent changes. Once the elastic region finishes, that would be the yield point of the material [15]. Past the yield point, plastic deformation begins. As the figure shows, this section is divided into two subparts. Strain hardening is the process where the material's strength increases as it is plastically deformed, due to the high density of dislocations, which improves the resistance towards deformation. The peak of the curve showcases the ultimate strength of the material. Pass that, necking begins, a phase where the deformation starts to localize in certain areas. As this goes on, at some point, rapture will take place, known as material failure.

Now, if we look at the area under the graph, that is equivalent to the toughness of the material. It is also measured by the amount of energy that a unit volume of the material has absorbed up to the failure point [15]. Furthermore, the shape of the curve can give insights into other properties of the material. Thus, a stress-strain curve provides insightful information about a material's properties. Therefore, they were used for studying our structures in this research.

Chapter 3

Methods

Numerous studies have focused on creating an isotropic model or rather, they have used patients and animals to further broaden our knowledge about how tissues function [17]. Although experimental setups provide insightful findings, they are often inconclusive and require significant resources. Thus, computational simulations have become vital to understanding the capabilities of our body. Molecular simulations offer a particularly advantageous tool, facilitating the information gathered experimentally and using it to create theoretical models to further understand the behavior of tissues at the molecular level.

3.1 Molecular Dynamics

Molecular dynamics (MD) simulations are widely used particle-based methods, due to their ability to provide a way to understand the dynamical properties of the system: transport coefficients, time-dependent responses to perturbations, rheological properties and spectra.

Molecular dynamics simulations consist of numerical solutions of the classical equations of motion by utilizing a set of initial conditions. These initial conditions are the initial positions $\{\mathbf{r}_i\}$ and the velocities of each particle $\frac{dr_i}{dt}$. The simulation accounts for all the particle-to-particle interactions denoted by $\mathbf{F}_i(t)$, where i ranges from 1 to n for a system containing n particles [17]. If we integrate these equations over time, we arrive at a continuous description of the behaviour and interactions of the molecules within the system.

3.2 Model

As mentioned in the introduction, we are using a simplified model of cartilage in this paper. The structure resembles only the structure of the collagen fibers of the cartilage, excluding the Glycosaminoglycans (GAGs) and all the other particles. The collagen fibers in cartilage are roughly 1 μm thick, thus σ is also 1 μm. The fibers contain 20 atoms and so the fibers is 20 μm long. The overall charge of the system is neutral. The orientation and number of fibers divided in each layer are based on the literature presented above, the resemblance being visible in the structure. Interconnectivity is present between the zones; details about that are explained in the next section. In this study, we utilized a coarse-grained model [18] within the LAMMPS Molecular Dynamics Simulator for cartilage simulations. The solvent within the simulation was

treated as an implicit good solvent due to the pairwise additive Lennard-Jones (LJ) interaction between polymer beads [19].

The particle interactions are modeled using a Lennard-Jones potential [17] with a cutoff set at $2^{1/6}\sigma$. Here, both the interaction energy ε and the particle size σ are set to 1.0. The Lennard-Jones potential is expressed as:

$$U_{LJ}(r) = 4\varepsilon \left[(\frac{\sigma}{r})^{12} - (\frac{\sigma}{r})^{6} \right] \tag{3.1}$$

The bonds between the particles are described by the FENE (Finite Extensible Nonlinear Elastic) potential. The FENE potential is given by:

$$V_{FENE}(r) = -0.5kR_0^2 ln \left[1 - \left(\frac{r}{R_0} \right)^2 \right], \quad \text{for } r \leq R_0 \tag{3.2}$$

The angle potential is calculated by taking the cosine of the angle formed by three atoms, multiplied by a constant that needs to be chosen by the user. This command allowed us to differentiate the layers of the structure by assigning a certain potential energy to the atom types in each layer. The top layer has K=50, the middle K=10 and the bottom one has K=50. The energy is given by:

$$E = K \left[1 + cos(\theta) \right] \tag{3.3}$$

Additionally, K acts as the stiffness coefficient of the fibers. Thus, higher k values make the system more resistant to deformation, requiring more energy to bend away from its original orientation.

3.3 Simulations Set-up

In order to analyze the properties of the structure, we performed mechanical deformation on slightly different versions of the structure, achieved by changing two parameters, namely the crosslinking density and the stiffness.

The crosslinking density is controlled with the command *fix...bond/create* [20]. It checks after a certain number of steps whether two atoms are close enough to form a bond between them (cross-link), and you can add a probability towards the command as well. Thus, to change the number of cross-linking bonds formed in each structure, we adjusted the probability of the command and the runtime of the simulations separately. There are three samples in total, two of which have the same length in terms of time steps (100k) but different probabilities of the cross-linking commands, namely, the low probability structure (LCL) has 0.1 for the same layers and 0.3 in between different layers. The base structure (MCL) has a probability within the same layer of 0.3 and 0.5 between different layers. The last structure has the same probabilities as the BS but has run for 300k time steps (HCL - high cross-linking density). The percentage of cross-linking is taken as the number of bonds created during the simulation in comparison to the total number of bonds at the end of the simulation.

Moreover, the angle potential's parameter K dictates the stiffness of the fibers. Thus, we

produced four more structures with increased stiffness. We chose the MCL and LCL structures as a reference point and we consider their stiffness as low (top layer - 50; middle layer - 10; bottom layer - 50). For each of the crosslinked structures, there are two more for which the stiffness was increased by 20 for every layer, except the middle layer. Table 3.1 displays all the structures with their descriptions. The deformation scripts include the command

Stiffness Crosslinking	50/10/50	70/50/70	90/70/90
0.1/0.3; 100k	X		
0.3/0.5; 100k	X	X	X
0.3/0.5; 300k	X	X	X

Table 3.1: All the structures with their crosslinking and stiffness properties

$fix...bond/break$, which goes through all the bonds at every time step and analyzes their lengths [20]. This method is used to model the dissolution of a polymer network due to deformation of the simulation box. If they become larger than a certain desired length (must be mentioned in the command), they are marked and set to be erased along with all the angle, dihedral, and improper interactions that the bond is part of.

3.4 Mechanical deformation and tests

Mechanical tests are simulations in which a constant deformation takes place for a certain number of steps. We have focused on compression on the z-axis and tension on the x-axis. The strain rate has been set to a certain value, and the deformation is continuous until the final timestep is completed. In order to make the deformations computational, we used the LAMMPS command $fix...deform$, which enables reduction or expansion of the simulation box [20].

The structure is allowed to relax just before it starts deforming, in order to equilibrate the system after the cross-linking procedure. For the tensile test, the strain rate was set to 0.000025 for 1.2 million steps. However, it is worth mentioning that after a certain strain, the data becomes redundant. The box was stretched by $0.001 * (units\ box)$. The compression test had the same strain rate, but it ran for 300k steps, due to the limitations of the size of the box. The reduction in the size of the box was set to $0.00055 * (units\ box)$. The box is compressed up to 82.5%.

These tests yield the data necessary to create the distribution between layers of the stress load on our structure. In addition, we collect information about the stress-strain curves alongside the mechanical properties of interest such as Young's modulus, yield point and toughness. Toughness is calculated by integration of the area under the stress-strain curve using the function $numpy.trapz$. The yield point is taken straight from the plots at the end of the linear relationship between the two. The ultimate tensile stress is extracted by taking the highest stress on the graph and looking for its associated strain.

The change in the orientation angle measurement has been conducted by the use of the initial

and final positions of the particles, which are saved during the simulation. Next, using *Python*, we compare the orientation angle of all the bonds within each layer with respect to a desired axis. Thus, we are able to observe how the deformation changed the orientation of the fibers. For the compression test, the orientation is based on the z-axis and for tensile, the x-axis was used.

Furthermore, the stress in the structure is analyzed layer by layer. Stress is the sum of the stresses in all three axes, thus, stress is distributed in all three axes for each layer. This way, we obtain a clear representation of which layer is responsible for sustaining the loads of the deformations.

3.5 Analysis

The structures simulated were first visually inspected using the $OVITO$ visualization software [21]. Analysis was achieved by making use of the *Python* programming language. Furthermore, plotting of the collected data was performed using the *numpy* and *matplotlib* packages. Numerical fitting of the obtained results was carried out with the $curve\ fit$ package from the *scipy.optimize* library, ensuring more reliable fits.

Chapter 4

Results and Discussion

As explained in the previous chapter, the three structures that have yielded the results have different cross-linking densities: LCL - 20.38%, MCL - 34.81% and HCL - 46.41%, as described in section 3.3. The density is calculated by taking the total number of bonds in the structure and the total number of bonds created during the crosslinking simulation and calculating what percentage of those bonds are due to the crosslinking procedure. As shown in Figure 4.1, as

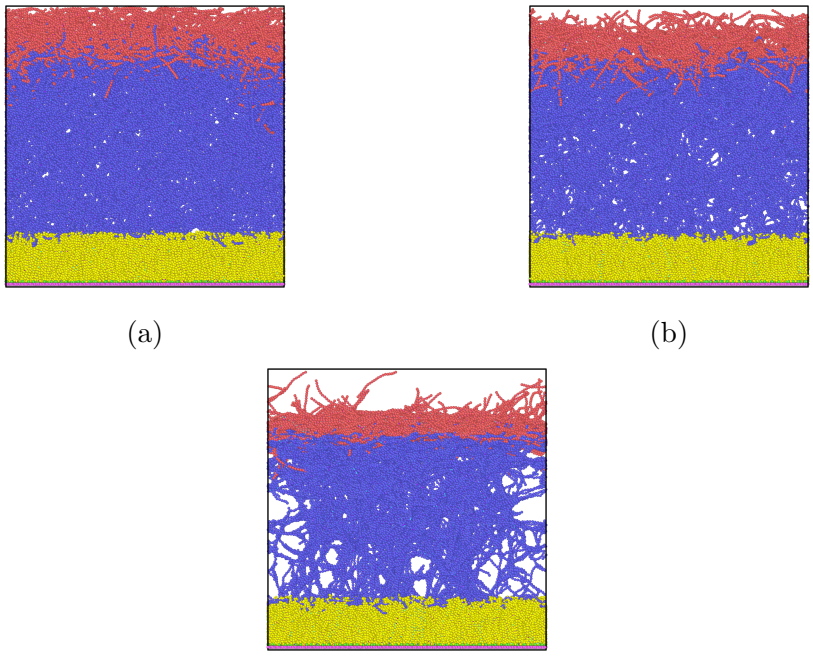

(a) (b)

(c)

Figure 4.1: Ovito representation of the three structures; a) LCL, b) MCL and c) HCL

the cross-linking (CL) density increases, the structure exhibits larger holes and occupies less space within the simulation box.

4.1 Stress Distribution/Mechanical properties/ Orientation Angle/ Stiffness

In this section, we review the plots and graphs generated from the data of our simulations. It is checked whether there are correlations observable between the different events that occurred during the deformations and associate them with existing literature.

4.1.1 Tensile

As explained in Chapter 3.2, a stress-strain curve is essential in determining the mechanical properties of a structure. In Figure 4.2, we observe the curves for all three samples (LCL, MCL, HCL).

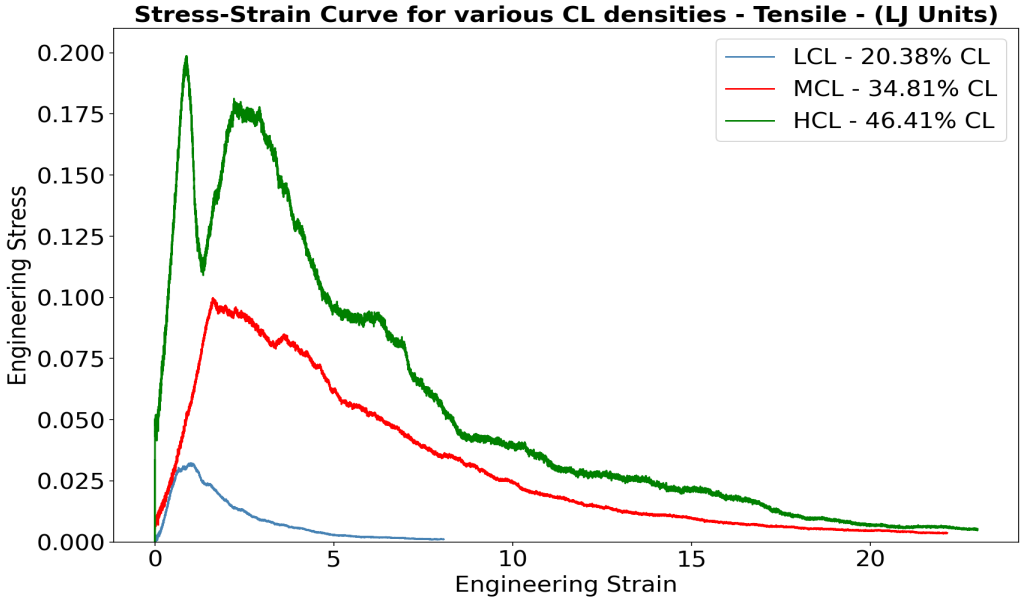

Figure 4.2: The stress-strain curve for the three structures for tensile deformation (LJ Units)

There is a clear differentiation between the samples in terms of the stress each one can sustain until failure is achieved. Shape-wise, all the structures exhibit similar curves, which suggests that an increase in crosslinking only affects the magnitude of stress that the structure can sustain. Certain mechanical properties are extracted from the tensile test. HCL shows the fastest linear increase in stress, having the steepest slope, indicating a more brittle behavior than the other structures. Its ultimate tensile strength (UTS) is relatively close to its yield point, meaning that the structure can't absorb much energy through plastic deformation [22]. Table 4.1 displays the mechanical properties extracted from the tests. As mentioned, as the CL density increases, the material becomes more brittle. HCL structure shares almost the same yield point stress as the ultimate tensile stress, showing extreme brittle behavior. LDL is the only structure that exhibits some plastic deformation, observed by the difference between its yield point and its ultimate tensile stress. Toughness increases rapidly with the increase in CL density.

(LJ units)	Yield σ	Yield ε	UTS	Toughness
LCL	0.0291	0.6636	0.0322	0.0725
MCL	0.0934	1.5965	0.0998	0.6792
HCL	0.1971	0.8884	0.1987	1.2529

Table 4.1: The mechanical properties for the three CL densities

There is a clear correlation between the increase in bonds being broken and the decrease in stress inside the material. Most of the broken bonds are located in the top and middle layers. During the relaxation time, there is already a sizable number of bonds that break, especially for the more dense structures. After the deformation begins, we can observe a slightly positive slope in the bond-breaking plots, which are presented in Figure 2 in the Appendix. Additionally, we can see that from the ultimate tensile stress point, there are too many bonds that are being broken by which releases stress. This is visible in Figure 2 in the Appendix. Thus, we believe the stress produced by the deformation becomes smaller compared to the stress released by the breakage of the bonds.

To analyze stress distribution, as mentioned in section 3.4, we divided the stress on each axis by each layer. Figures 4.3, 4.4, and 4.5 suggest that most of the load on the x-axis is sustained by the bottom layer for all the structures. The particles feel stress along the other axes as well; however, their magnitude is insignificant compared to that in the direction of the deformation.

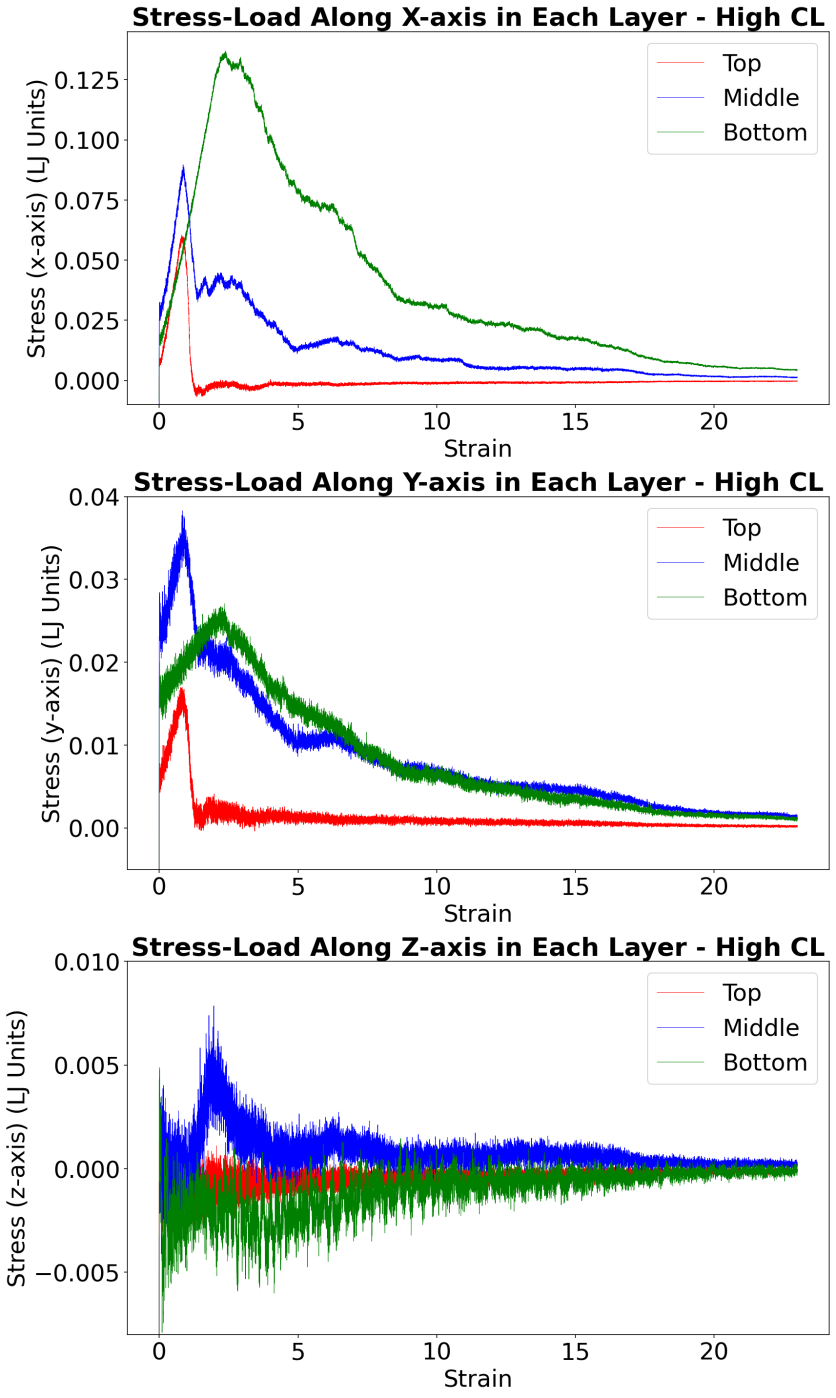

Figure 4.3: The stress-strain curve on every layer and axis for the HCL structure during Tensile deformation

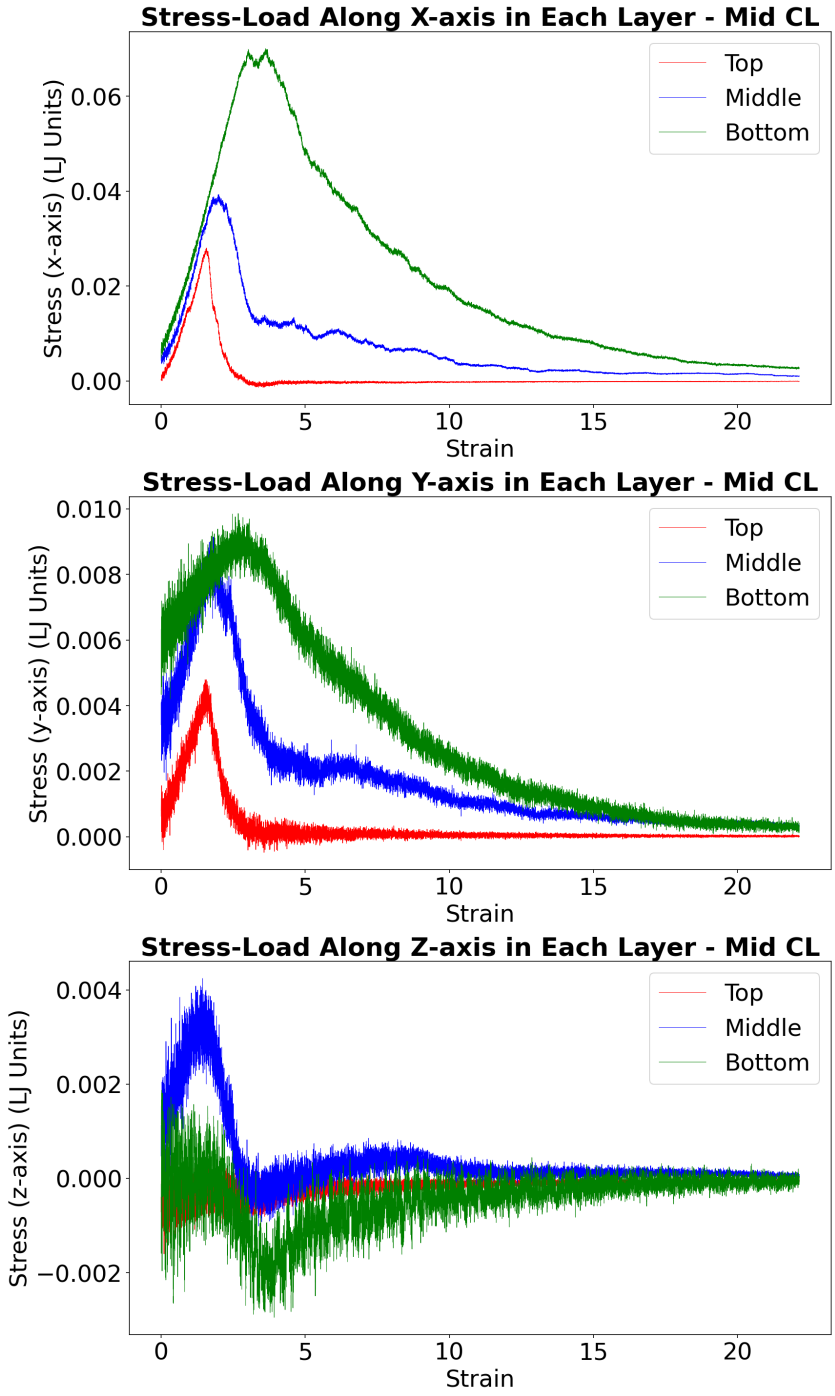

Figure 4.4: The stress-strain curve on every layer and axis for the MCL structure during Tensile deformation

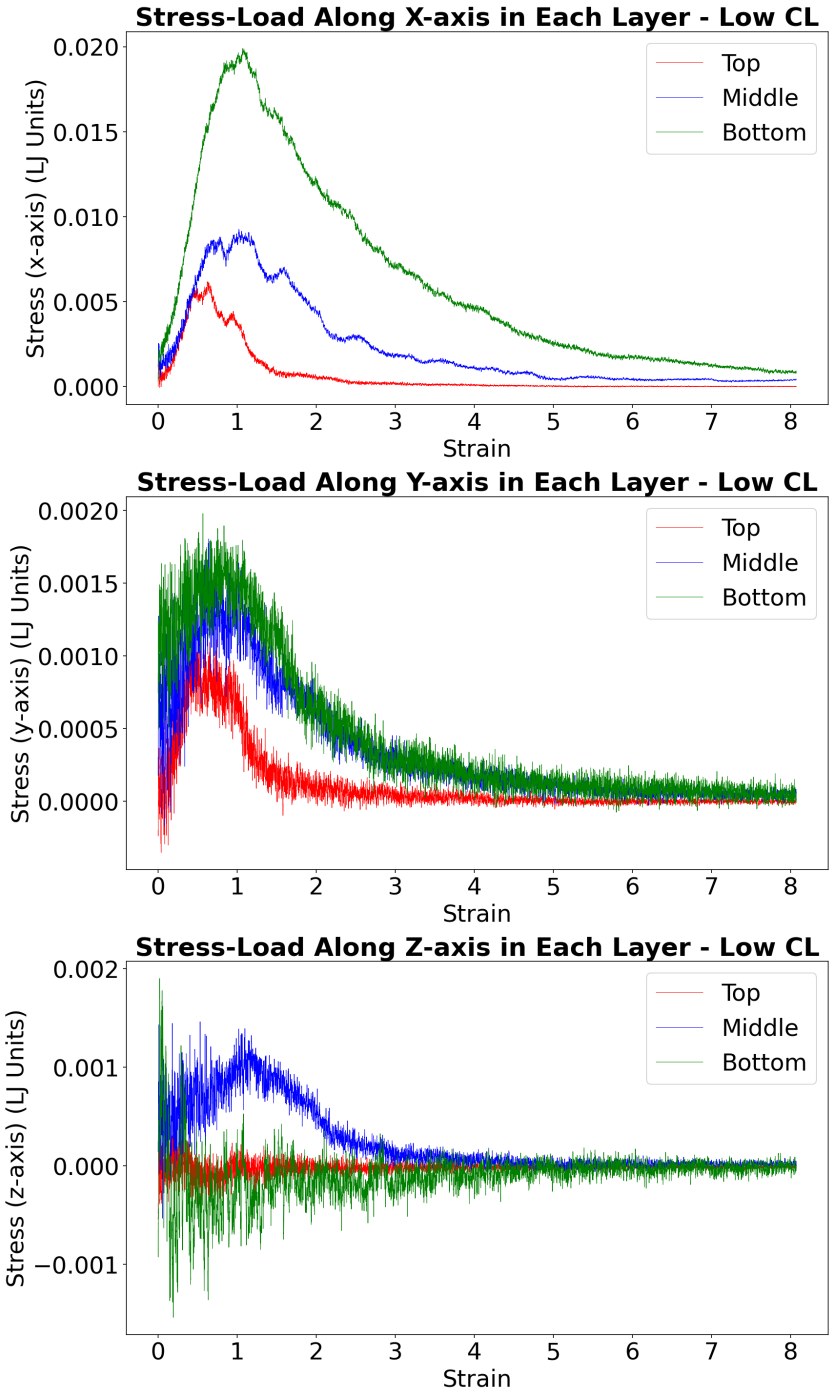

Figure 4.5: The stress-strain curve on every layer and axis for the LCL structure during Tensile deformation

The fiber orientation plots, presented in Figure 4.6, show that the vertical layer experienced the most change during the deformation. We observe a flatter bell curve distribution in the orientation of the fibers in the bottom layer. This is most accentuated at the lower CL densities, since the structure has less resistance against deformation. Additionally, flattening occurs in the middle layer, mostly in the LCL structure. It would seem that the layer that sustains the

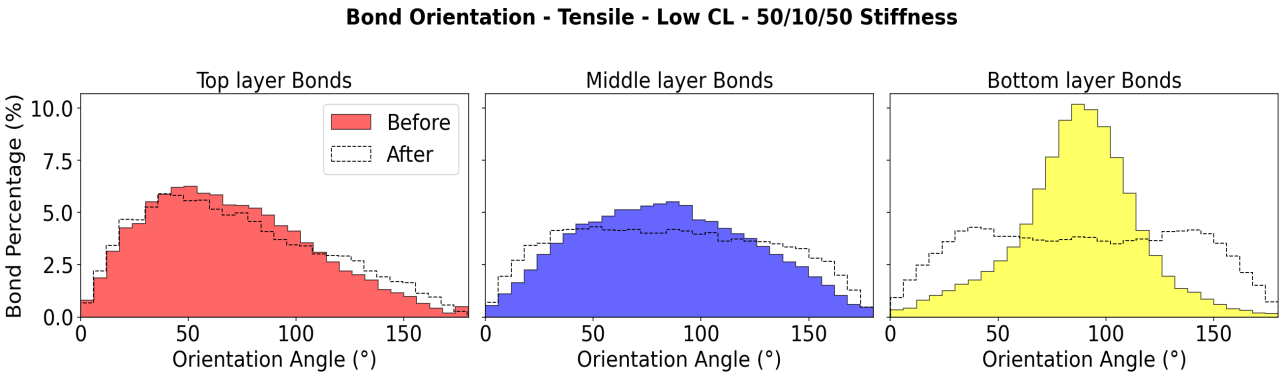

Figure 4.6: Plot of the orientation angle of LCL for each layer, before and after tensile deformation.

highest amplitude of stress is the one that shifts its orientation the most. However, we think that there is not enough evidence to support a correlation between these events, especially given the fact that the orientation angle is calculated right at the end of the deformation and not throughout it. On the other hand, most of the fibers in the deep zone are approximately at 90° from the direction of the deformation. Literature on isotropic and anisotropic structures tells us that the orientation of the fiber impacts the load it will experience, as suggested here [23,24]. Fibers perpendicular and parallel to the deformation will experience most of the stress and around $30° - 45°$ the least [24], suggesting that the methodology of our tests is correct. Another research paper found that in an isotropic system, the dependency of the Young modulus of a composite is U-shaped, as seen in Figure 1 in the Appendix. It also mentions that the results from the simulations differ from the experimental cases [25].

Interestingly, the top layer (the most aligned with the deformation) shows the least amount of stress. One explanation could be that the number of fibers present in that layer is significantly lower than in the other layers. The deep zone has almost triple the particles as the superficial zone and since the stress at every timestep is the sum of the stress of all particles, it could be a reason for these results. Another one could be that during the deformation, most of the bonds that broke are from the superficial layer for all structures. The fibers from the deep zone experience almost no breakage compared to the top layer.

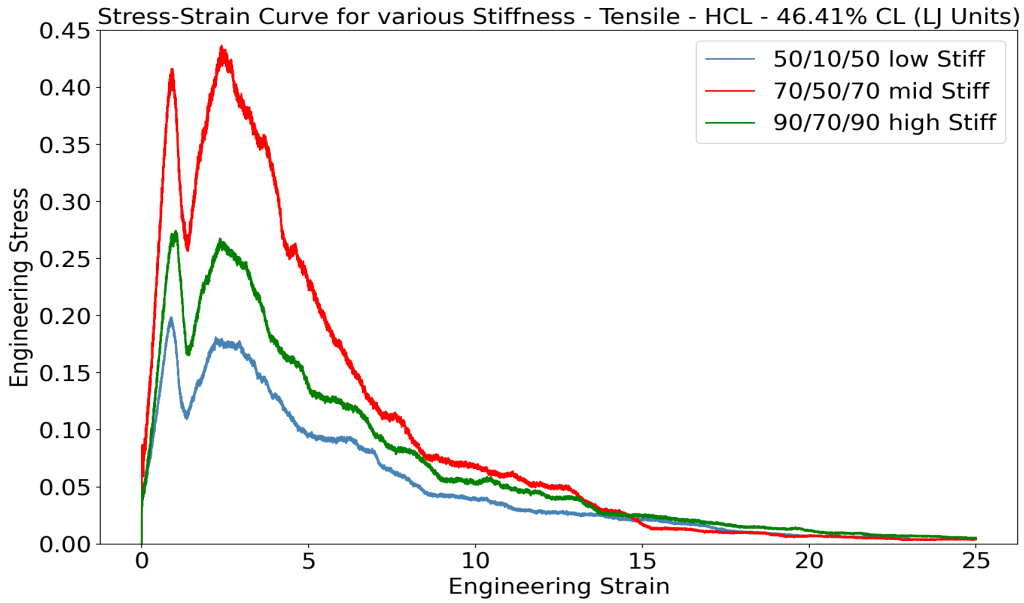

(a)

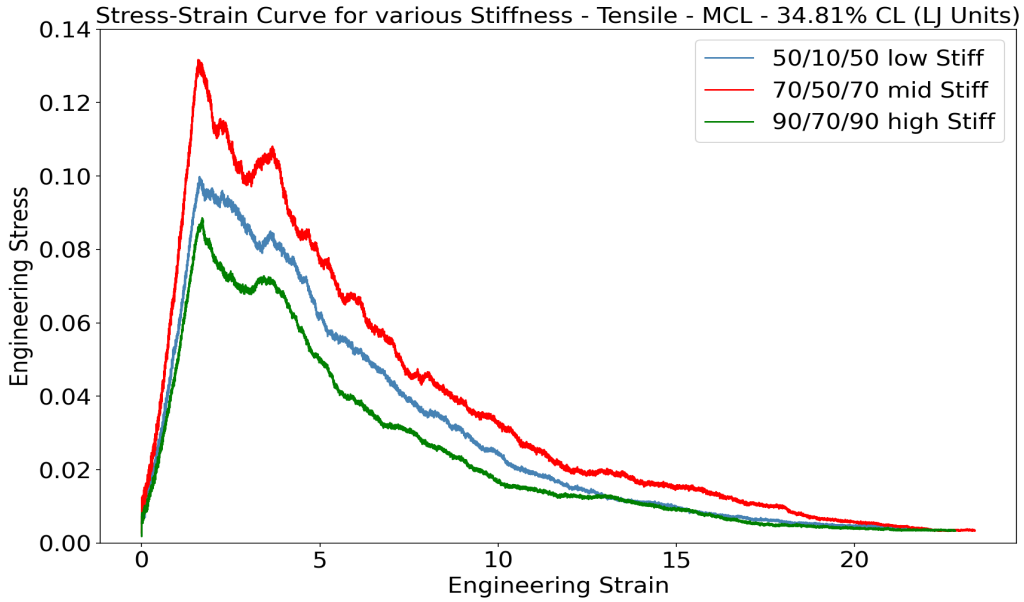

(b)

Figure 4.7: The stress-strain curves for different stiffnesses of the a) HCL and b) MCL structures during tensile deformation

Moreover, changing stiffness yielded unexpected results. We have run deformation simulations for 3 stiffnesses for the MCL and HCL structures. They are presented in Figure 4.7. The straightforward thinking would suggest that more particles/bonds result in higher amplitudes of stress. However, we found that the maximum stress was achieved by the intermediate stiffness, not the highest. Additionally, for the MCL structure, the highest stiffness showed a smaller toughness than the low stiffness model. Literature suggests that during deformation, some materials experience enough displacement that the orientation of their fibers changes so that they can withstand the deformation better [26]. Thus, when stiffness is increased over a

certain threshold, the system is not capable of deforming properly to allow for an improved resistance against the tensile test.

4.1.2 Compression

The compression test, as mentioned previously, involves some limitations in the simulation parameters. The total strain is constrained by the size of the simulation box. Thus, the stress-strain curve for the compression test has a different morphology, represented in Figure 4.8. The plot shown has only the data from the second half of the deformation due to the small

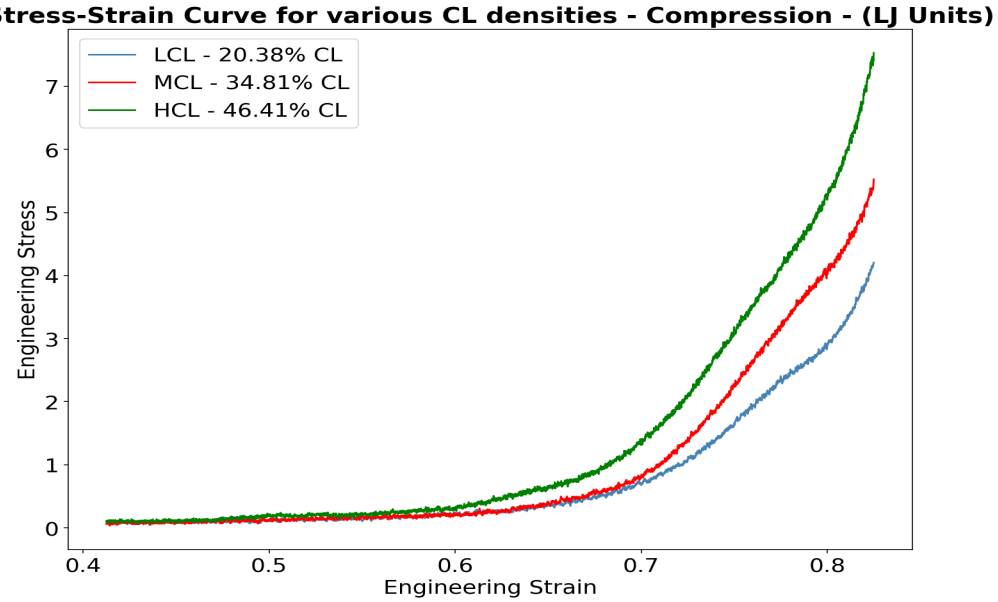

Figure 4.8: Stress-strain curves of the three structures

amplitude of stress in the first half of the data. This way, we concentrate only on the relevant information. As expected, the structures with higher CL densities exhibit a higher stress load. Due to the nature of the plot, the only mechanical property we can accurately extract is a relative toughness between the three samples. Table 4.2 showcases these results.

	Toughness (LJ units)
LCL	0.3380
MCL	0.4310
HCL	0.5979

Table 4.2: The toughness of the three structures

During tensile deformation, the majority of broken bonds occur within the top layer, whereas in compression testing, most broken bonds are concentrated between the top and middle zones. It would seem that, even though the number of broken bonds is fairly large during the compression test, the total stress produced by the deformation is higher than the one released by the breaking of bonds. Thus, we think that there might be a relationship between these two events; however,

more experiments need to be conducted.

Moreover, the stress distributions within each layer for compression are shown in the Figure 4.9, 4.10 and 4.11. Again, the fibers from the deep zone experience the most stress in the z-axis, which aligns with the literature.

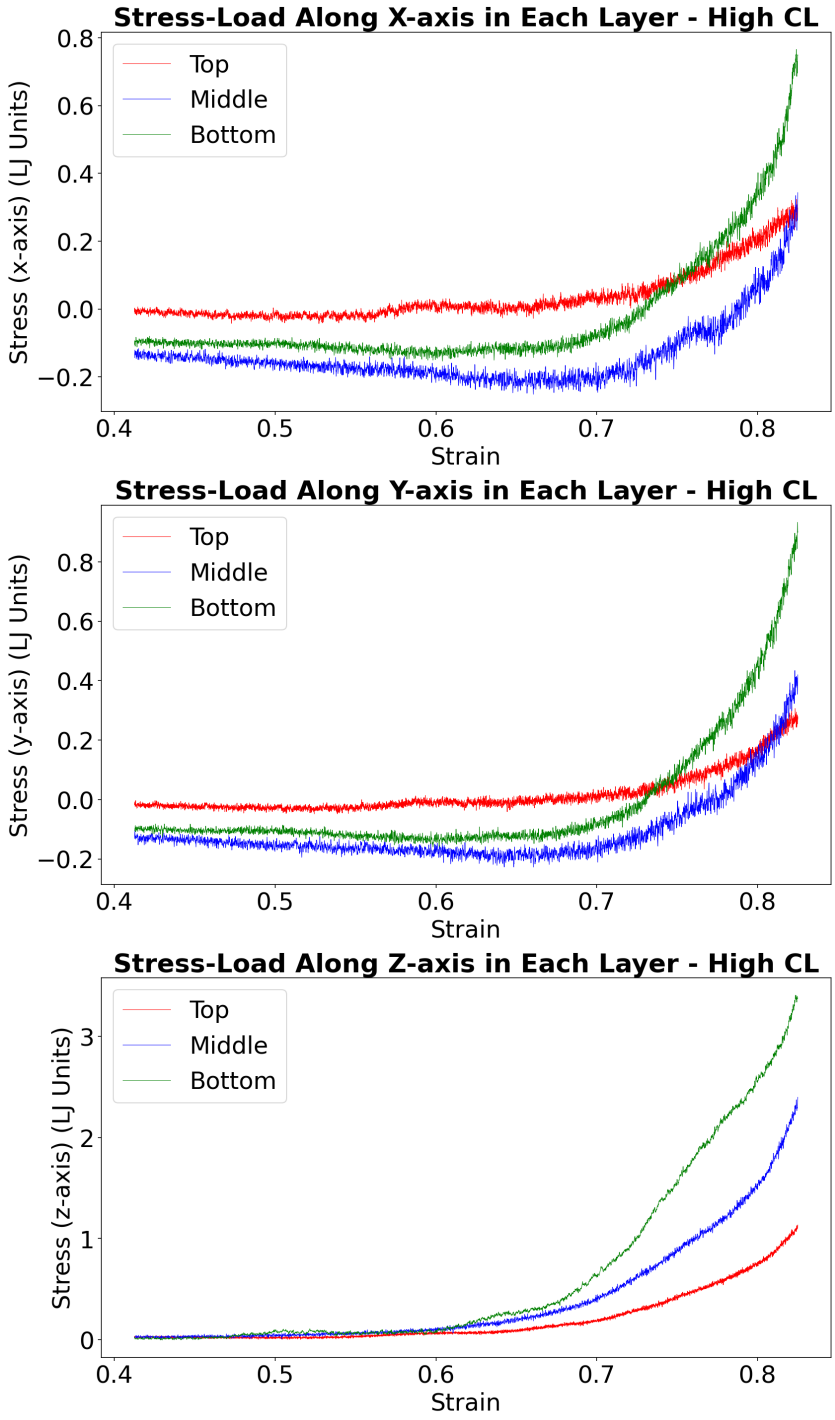

Figure 4.9: The stress-strain curve on every layer and axis for the HCL structure during Compressive deformation

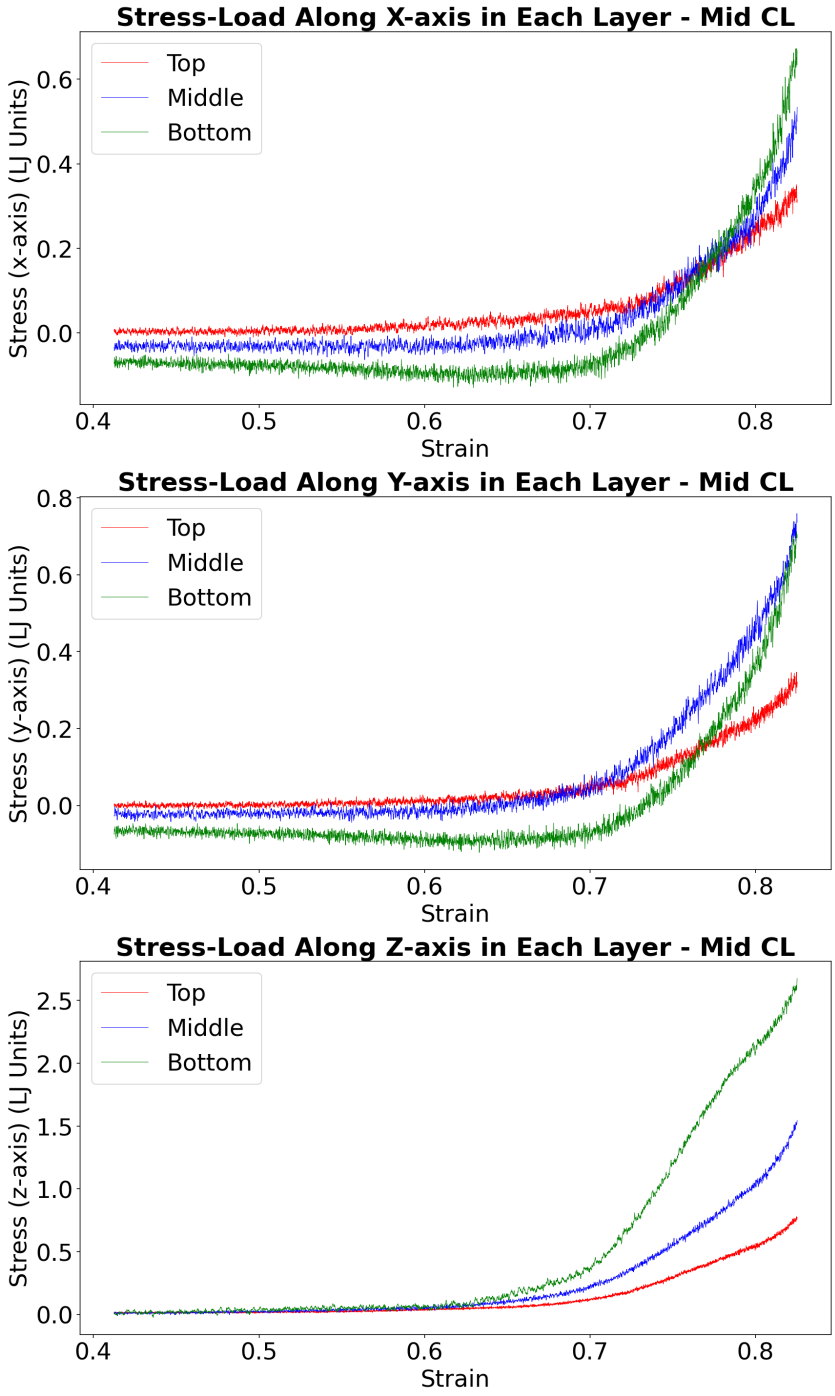

Figure 4.10: The stress-strain curve on every layer and axis for the MCL structure during Compressive deformation

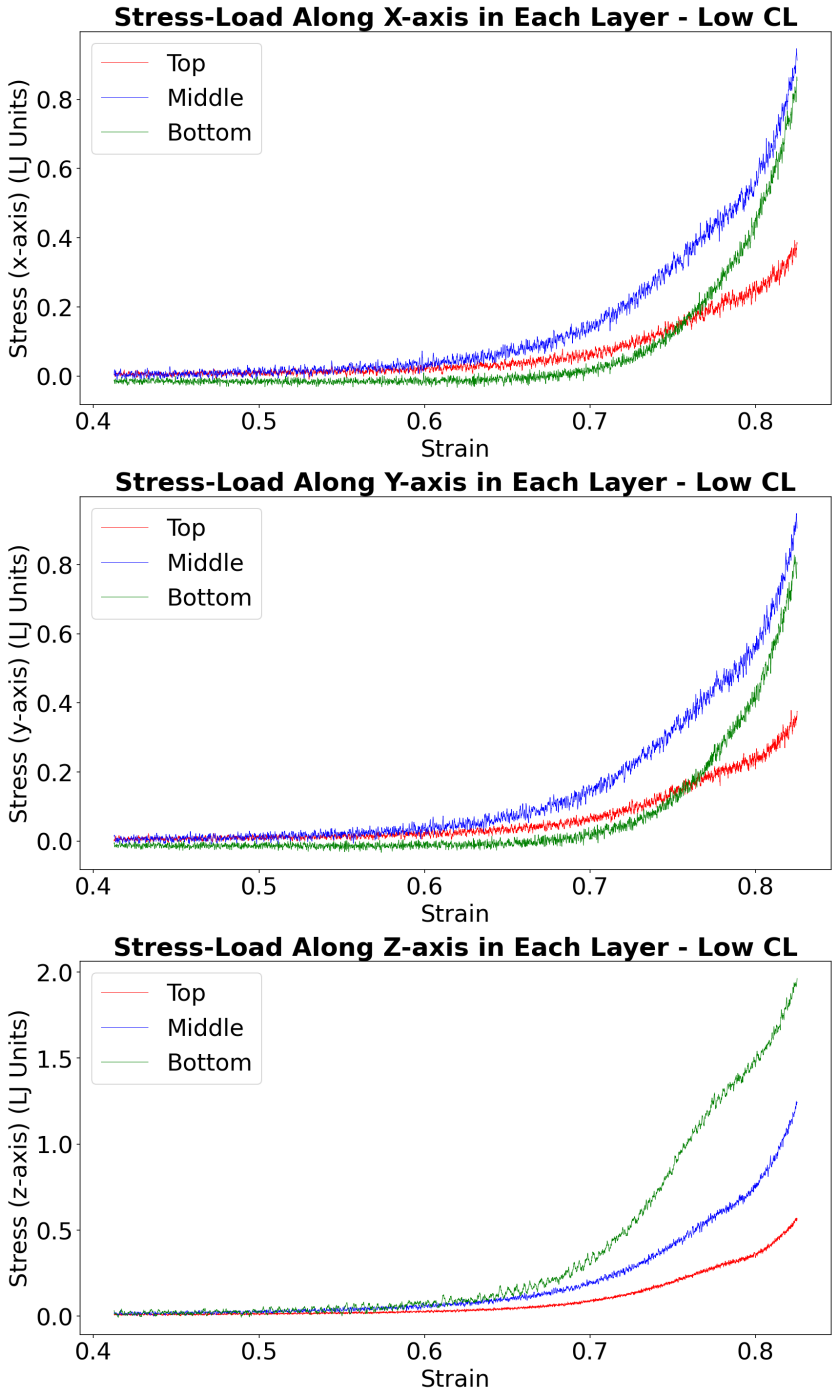

Figure 4.11: The stress-strain curve on every layer and axis for the LCL structure during Compressive deformation

This behavior can be observed in all the structures, only at different magnitudes of stress due to their various CL densities. The stress in directions other than the deformation is more noticeable compared to the tensile tests. Interestingly, the middle zone seems to experience the largest amount of stress in the x and y axes. This occurs only for LCL and MCL. We think that due to the decreased number of bonds in the middle layer, that part of the system becomes less rigid and therefore has more freedom of movement. This is backed up by the bond orientation

plots. In Figure 4.6, there is a noticeable change in the orientation of the bonds within the middle layer.

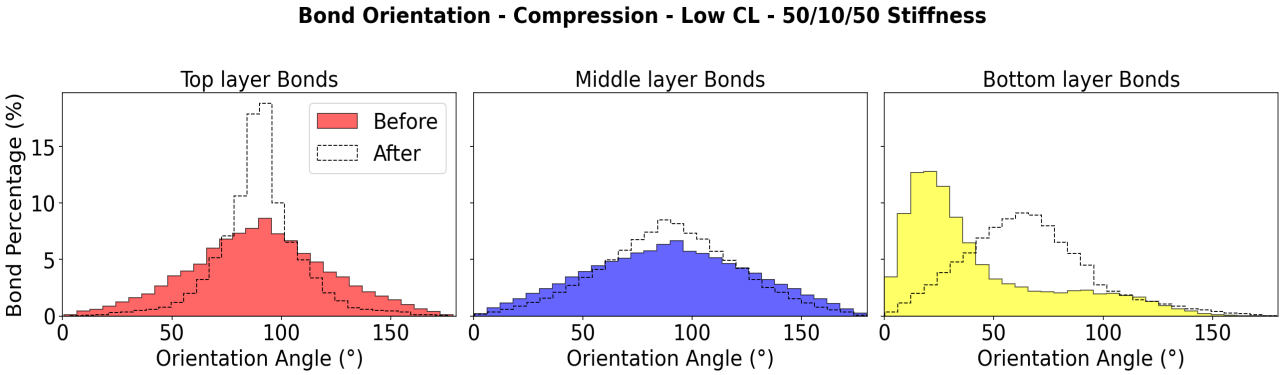

Figure 4.12: Plot of the orientation angle of LCL for each layer, before and after compression

Consequently, some of them reoriented more towards 90°, which results in higher stress loads. Moreover, as the density of CL is increased, producing a sizable increase in rigidity in the middle layer, we observe that the magnitude of the stresses in the x and y axes does not grow with the increase number of bonds, rather it stays the same or decreases.

Changing the stiffness of the MCL and HCL during the compression test produced expected results, unlike the tensile test. The difference between each structure is the magnitude of stress, presented in Figure 3 in the Appendix. The discrepancy between the two tests, we assume, is due to the different intensities of the tests. The tensile test runs for longer and has a higher strain rate. Furthermore, the compression test has limited strain rates as well as the timespan of the simulation.

4.2 Ethics

In this type of research, where all of the analysis and practices were done only on a computer, it is challenging to bring ethics in the discussion. In terms of GenAI usage, it was only used in two python codes, mainly to improve the quality of the resulting plots. Besides that, the open AI was not used for paraphrasing or generating text for the thesis. My research is morally acceptable due to its main purpose, that is to demonstrate that the future research of human tissue is in the hands of computational simulations.

Chapter 5

Conclusion

This study attempted to create and analyze a simplified model of cartilage based on its mechanical properties and behavior, with the purpose of better understanding how to adapt a biological tissue to a simulation in order to further use this technology in future research. Molecular dynamics simulations were employed to explore these properties using a coarse-grained model. The analysis focused on creating multiple structures by changing parameters such as CL density and stiffness, only to subject them to mechanical tests, thus observing their behavior.

Regarding the change in CL density, as it increased, the structures exhibited a more brittle behavior, noted by how close the values for ultimate tensile stress and the yield point were in the tensile test. Such a result expresses the small amount of plastic deformation these structures can absorb until failure [23]. Healthy cartilage can sustain high loadings and while it is able to undergo plastic deformation, that may lead to permanent damage to the tissue [26]. Additionally, the compression test revealed consistent results; the increase in CL density resulted in a higher amplitude of stress. The bond-breaking analysis gave a different perspective on how the stress was released during the deformation, backing up the stress-strain curves. The stress distribution plots exhibited that the bottom layer sustained the most stress in the direction of the deformation for both the compression and tensile test. This partially aligns with the literature. In the healthy cartilage, the deep zone sustains most of the load during compression, while the superficial layer, which is aligned in the direction of the uniaxial tensile deformation, is responsible for the loading. Additionally, literature also suggests that perpendicular fibers to the direction of the deformation experience significantly higher stress levels than the others. This could result from poor implementation of deformation. The orientation angle plots revealed the final orientation of the fibers compared to the axis of deformation. It revealed another insight into the magnitude of change during the deformation. At lower CL densities, all three layers show a reasonable change in orientation. This is important as literature explains that biological tissues tend to slightly reorient their structure during deformation to better sustain the loads [27]. Moreover, changing the stiffness of the structure backed up the importance of the ability of a tissue's fibers to move towards an ideal position to withstand the pressure. The mechanical tests revealed that the medium stiffness yielded the highest mechanical performance. The highest stiffness was placed second and even last for the MCL structure.
In conclusion, this study represents a solid start in recreating and testing a simulated biological tissue. The results proved the simplicity of the used model, but at the same time, it showed the key aspects of the real cartilage.

In future research, by systematically adding GAGs along with their charges, we can gain a more accurate insight into the true mechanical properties of the tissue. Subsequently, this new structure can undergo a creep or relaxation test to extract the visco-elastic properties of the material. This is a key property of the cartilage as it allows it to absorb shock and distribute loads [28]. Furthermore, the flow of nutrients is crucial for the survival of the cartilage. Thus, a permeability test could be conducted to ensure that the model matches the real tissue. These future studies can employ advanced simulation techniques and experimental methods to validate the refined models. By extending the investigation to include more samples with smaller discrepancies between each other, a more comprehensive picture can be developed. These efforts will help enhance our understanding of the human body, how all the small parts of our tissues interact with each other, thus developing new applications in nanotechnology, materials engineering and biomedical engineering.

References

[1] C. E. Korenczuk et al., "Isotropic Failure Criteria Are Not Appropriate for Anisotropic Fibrous Biological Tissues," Journal of Biomechanical Engineering, vol. 139, no. 7, pp. 0710081–07100810, Jul. 2017, doi: https://doi.org/10.1115/1.4036316.

[2] B. Bordoni and M. Varacallo, "Anatomy, Tendons," Nih.gov, 2019. https://www.ncbi.nlm.nih.gov/books/NBK513237/.

[3] G. Donald Whedon and R. Proulx Heaney, "Bone - Bone morphology," Encyclopædia Britannica. Feb. 28, 2019. Available: https://www.britannica.com/science/bone-anatomy/Bone-morphology.

[4] T. Newman, "Cartilage damage: Symptoms, causes, diagnosis, and treatment," www.medicalnewstoday.com, Dec. 15, 2017. https://www.medicalnewstoday.com/articles/171780what-is-cartilage.

[5] W. Zuidema et al., "Five Ways in Which Computational Modeling Can Help Advance Cognitive Science: Lessons From Artificial Grammar Learning," Topics in Cognitive Science, vol. 12, no. 3, pp. 925–941, Oct. 2019, doi: https://doi.org/10.1111/tops.12474.

[6] J. Nachtsheim, G. Dursun, B. Markert, and M. Stoffel, "Chondrocyte colonisation of a tissue-engineered cartilage substitute under a mechanical stimulus," Medical Engineering & Physics, vol. 74, pp. 58–64, Oct. 2019, doi: https://doi.org/10.1016/j.medengphy.2019.09.022.

[7] X. Wang, C. P. Neu, and D. M. Pierce, "Advances toward multiscale computational models of cartilage mechanics and mechanobiology," Current Opinion in Biomedical Engineering, vol. 11, pp. 51–57, Sep. 2019, doi: https://doi.org/10.1016/j.cobme.2019.09.013.

[8] E. Belluzzi, S. Todros, A. Pozzuoli, P. Ruggieri, E. L. Carniel, and A. Berardo, "Human Cartilage Biomechanics: Experimental and Theoretical Approaches towards the Identification of Mechanical Properties in Healthy and Osteoarthritic Conditions," Processes, vol. 11, no. 4, p. 1014, Apr. 2023, doi: https://doi.org/10.3390/pr11041014.

[9] W. Ahmed and D. A. Phoenix, Advances In Medical And Surgical Engineering. S.L.: Elsevier Academic Press, 2020.

[10] S. R. Goldring and M. B. Goldring, "Changes in the osteochondral unit during osteoarthritis: structure, function and cartilage–bone crosstalk," Nature Reviews Rheumatology, vol. 12, no. 11, pp. 632–644, Sep. 2016, doi: https://doi.org/10.1038/nrrheum.2016.148.

[11] V. Vitek, "Mechanical Property - an overview — ScienceDirect Topics," www.sciencedirect.com, 2009. https://www.sciencedirect.com/topics/materials-science/mechanical-property.

[12] J. Eschweiler et al., "The Biomechanics of Cartilage—An Overview," Life, vol. 11, no. 4, p. 302, Apr. 2021, doi: https://doi.org/10.3390/life11040302.

[13] A. J. Sophia Fox, A. Bedi, and S. A. Rodeo, "The Basic Science of Articular Cartilage: Structure, Composition, and Function," Sports Health: A Multidisciplinary Approach, vol. 1, no. 6, pp. 461–468, Nov. 2009, doi: https://doi.org/10.1177/1941738109350438.

[14] Dr. Buckwalter, Dr. Mow, and Dr. Ratcliffe, "Restoration of Injured or Degenerated Articular Cartilage : JAAOS - Journal of the American Academy of Orthopaedic Surgeons," LWW, 2025. https://journals.lww.com/jaaos/fulltext/1994/07000/restoration of injured or degenerated articular.2.aspx (accessed Jun. 19, 2025).

[15] S. S. Murugan, "(PDF) Mechanical Properties of Materials: Definition, Testing and Application," ResearchGate, 2020. https://www.researchgate.net/publication/344287957 Mechanical Properties of Materials Definition Testing and Application.

[16] Tudelft.nl, 2025. https://ocw.tudelft.nl/wp-content/uploads/stressstraincomplete.png.

[17] M. C. van Turnhout, H. Schipper, B. van Lagen, H. Zuilhof, S. Kranenbarg, and J. L. van Leeuwen, "Postnatal development of depth-dependent collagen density in ovine articular cartilage," BMC Developmental Biology, vol. 10, no. 1, p. 108, 2010, doi: https://doi.org/10.1186/1471-213x-10-108.

[18] T. Casalini, "Coarse Grained Model - an overview — ScienceDirect Topics," www.sciencedirect.com, 2020. https://www.sciencedirect.com/topics/materials-science/coarse-grained-model.

[19] G. Reddy and A. Yethiraj, "Implicit and Explicit Solvent Models for the Simulation of Dilute Polymer Solutions," Macromolecules, vol. 39, no. 24, pp. 8536–8542, Oct. 2006, doi: https://doi.org/10.1021/ma061176+.

[20] A. P. Thompson, H. M. Aktulga, R. Berger, D. S. Bolintineanu, W. M. Brown, P. S. Crozier, P. J. in 't Veld, A. Kohlmeyer, S. G. Moore, T. D. Nguyen, R. Shan, M. J. Stevens, J. Tranchida, C. Trott, S. J. Plimpton, LAMMPS - a flexible simulation tool for particle-based materials modeling at the atomic, meso, and continuum scales, Comp Phys Comm, 271 (2022) 10817.

[21] A. Stukowski. Visualization and analysis of atomistic simulation data with ovito– the open visualization tool. Modelling and simulation in materials science and engineering, 18(1):015012, 2009. https://doi.org/10.1016/j.cpc.2021.108171.

[22] Shane, "Understanding Ultimate Tensile Strength: A Technical Deep Dive - MFG Shop," MFG Shop, May 29, 2025. https://shop.machinemfg.com/understanding-ultimate-tensile-strength/ (accessed Jun. 19, 2025).

[23] T. Heitkamp et al., "Stress-adapted fiber orientation along the principal stress directions for continuous fiber-reinforced material extrusion," Progress in Additive Manufacturing, vol. 8, no. 3, pp. 541–559, Sep. 2022, doi: https://doi.org/10.1007/s40964-022-00347-x.

[24] U. Sharan Gupta, A. Dharkar, M. Dhamarikar et al., "Study on the effects of fiber orientation on the mechanical properties of natural fiber reinforced epoxy composite by finite element method," Materials Today: Proceedings, vol. 45, pp. 7885–7893, 2021, doi: https://doi.org/10.1016/j.matpr.2020.12.614.

[25] H. W. Wang, H. W. Zhou, L. L. Gui, H. W. Ji, and X. C. Zhang, "Analysis of effect of fiber orientation on Young's modulus for unidirectional fiber reinforced composites," Composites Part B: Engineering, vol. 56, pp. 733–739, Jan. 2014, doi: https://doi.org/10.1016/j.compositesb.2013.09.020.

[26] M. Jaspers, S. L. Vaessen, P. van Schayik, D. Voerman, A. E. Rowan, and P. H. J. Kouwer, "Nonlinear mechanics of hybrid polymer networks that mimic the complex mechanical environment of cells," Nature Communications, vol. 8, no. 1, May 2017, doi: https://doi.org/10.1038/ncomms15478.

[27] M. Adouni, F. Alkhatib, A. Gouissem, and T. R. Faisal, "Knee joint biomechanics and cartilage damage prediction during landing: A hybrid MD-FE-musculoskeletal modeling," PLOS ONE, vol. 18, no. 8, pp. e0287479–e0287479, Aug. 2023, doi: https://doi.org/10.1371/journal.pone.0287479.

[28] J. Desrochers, M. W. Amrein, and J. R. Matyas, "Viscoelasticity of the articular cartilage surface in early osteoarthritis," Osteoarthritis and Cartilage, vol. 20, no. 5, pp. 413–421, May 2012, doi: https://doi.org/10.1016/j.joca.2012.01.011.

Appendix

This section contains additional plots that support and expand upon the analysis presented in the main text. Specifically, the figures illustrate key aspects such as the breakage of molecular bonds, variations in orientation angles, and the distribution of stress across individual layers of the structure. These visualizations provide further insight into the mechanics and structural behavior discussed throughout the thesis.

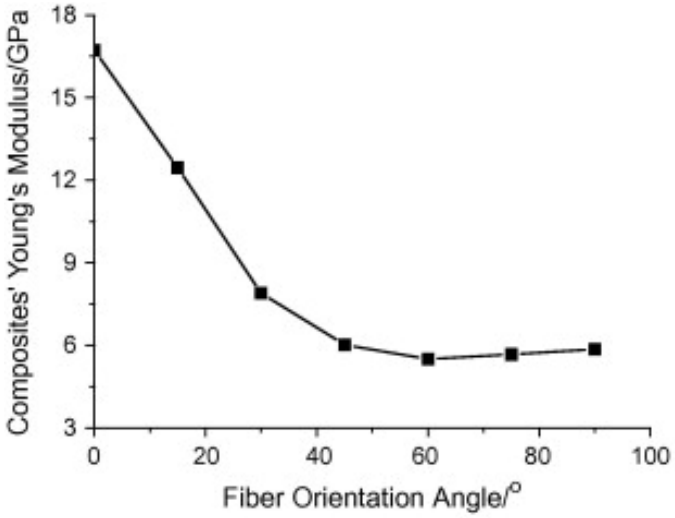

Figure 1: U-shaped dependency of the Young modulus of composites on the fiber orientation angle

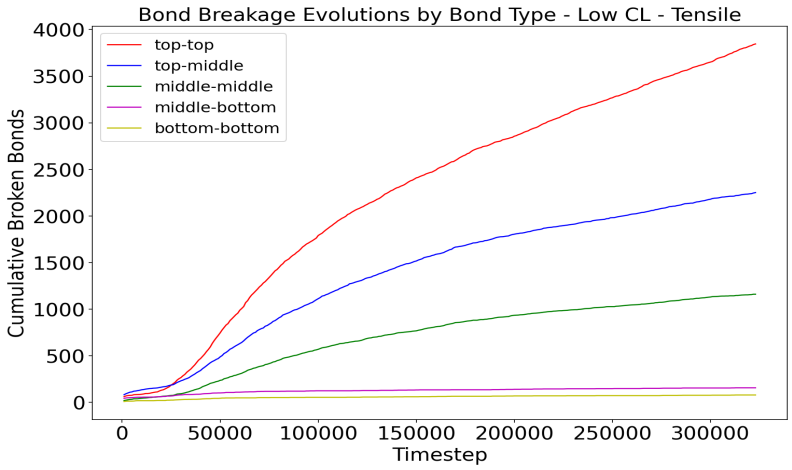

(a)

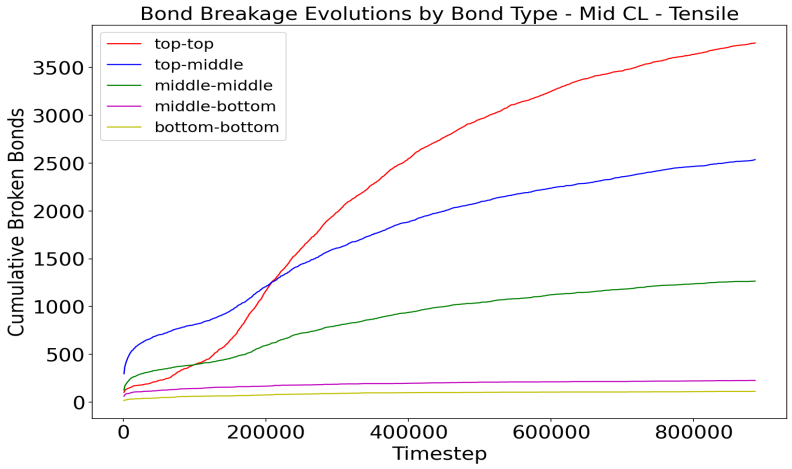

(b)

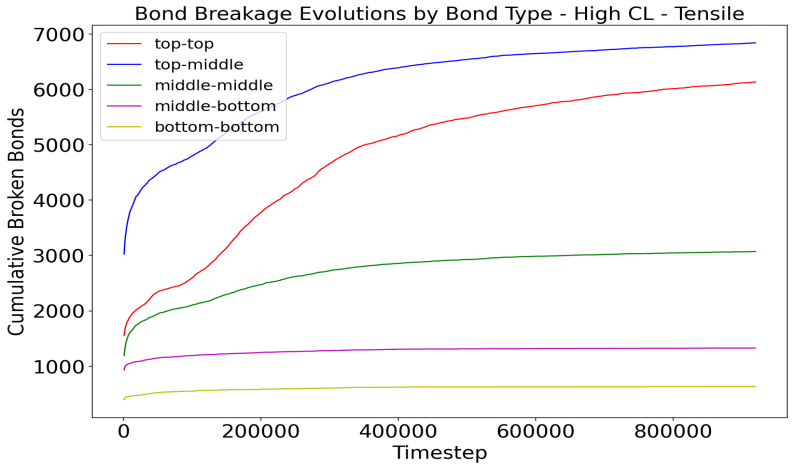

(c)

Figure 2: The evolution of bond-breakage during Tensile deformation for the three CL density structures: a) LCL, b)MCL, c)HCL

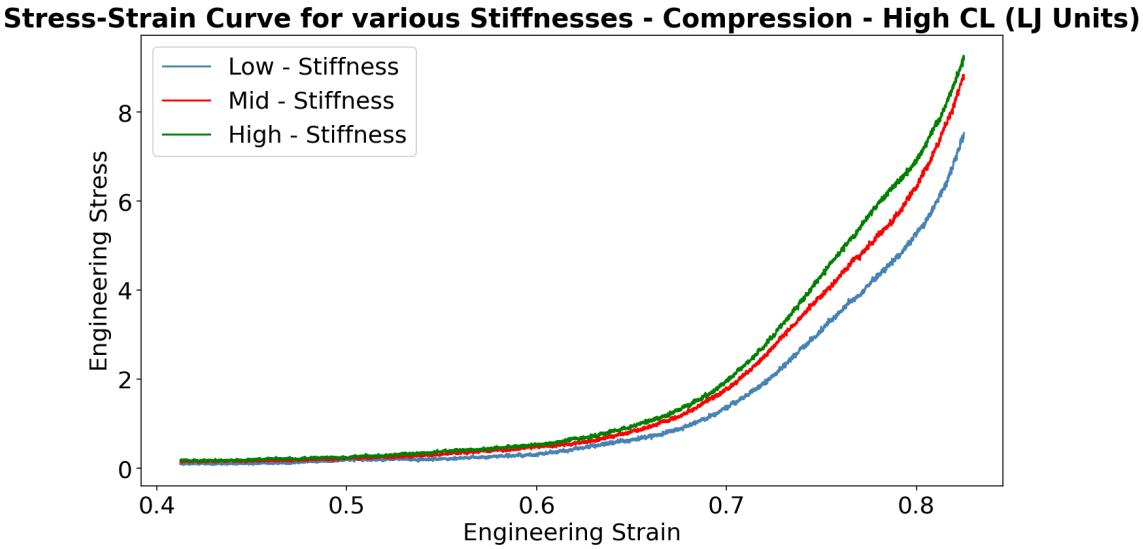

(a)

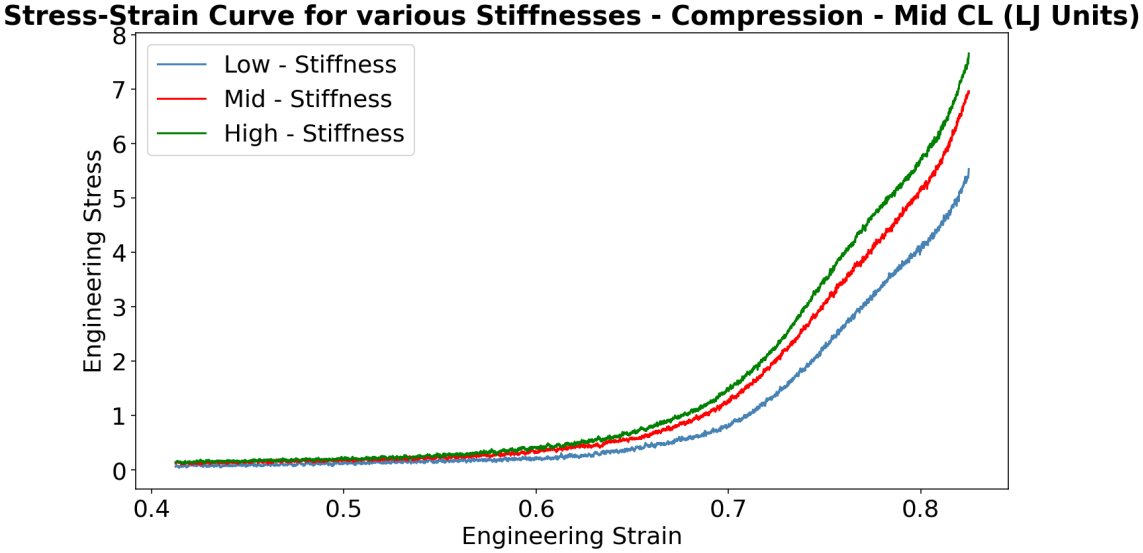

(b)

Figure 3: The stress-strain curves for different stiffnesses of the a) HCL and b) MCL structures during Compressive deformation